Modifying interprotein interactions for controlling heat-induced protein gelation

Sugam Kumar [1,2,*] Debasish Saha [1] and Vinod K. Aswal [1,2,†]
[1]Solid State Physics Division, Bhabha Atomic Research Centre, Mumbai 400 085, India
[2]Homi Bhabha National Institute, Mumbai 400 094, India

(Received 13 September 2022; accepted 4 January 2023; published 20 January 2023)

Globular proteins undergo heat-induced denaturation and eventually gelation at significantly elevated temperatures. The present study provides pathways to control temperature-driven protein gelation, having potential applications in a wide range of fields, from medicine to cosmetics to the food industry. The sol-gel transitions have been directed via modifying interprotein (electrostatic and hydrophobic) interactions by complexation of protein with amphiphiles. The heat-induced gelation of bovine serum albumin protein (anionic) is prevented in the presence of anionic sodium dodecyl sulfate (SDS) surfactant without significantly altering its native conformation. The specific binding of SDS monomers on the oppositely charged sites of protein increases the electrostatic repulsion between protein molecules, thereby suppressing the protein gelation. On the other hand, incorporating nonionic decaoxyethylene $n-$dodecylether ($C_{12}E_{10}$) surfactant along with ionic surfactant reverses this scenario, and the solution state of the bovine serum albumin-SDS system undergoes gelation. The preferential binding of SDS with $C_{12}E_{10}$ nonionic surfactant forms detached mixed micelles, resulting in the release of the SDS monomers from protein, hence reverting the SDS-induced prevention of protein gelation. The results are counterintuitive and explained based on the interplay of hydrophobic and electrostatic interactions among protein molecules, as probed by small-angle neutron scattering, dynamic light scattering, and rheology.

DOI: 10.1103/PhysRevMaterials.7.015601

I. INTRODUCTION

Proteins are one of the most versatile biomolecules, which participate in almost all the essential functions of living creatures. The function of the globular proteins is determined by their unique three-dimensional folded structure, which is known to be perturbed by specific physicochemical parameters such as temperature, pH and/or the presence of additives, etc. [1–4]. The heating of globular protein solution leads to an irreversible thermal process, which first denatures the protein, then aggregates these denatured proteins, and finally gives rise to protein gelation by forming intermolecular network structure above the gelation temperature (T_G) [5,6]. The protein gelation may be undesired in many cases, such as those leading to disruption of biological processes or deliberate for specific applications, e.g., in food, the biomedical industry, etc. [6–11]. Nevertheless, it is always worthwhile gaining control over the protein gelation for its desirable and effective utilization [12,13].

The process of protein gelation is decided by the interplay of inter- and intraprotein interactions, with electrostatic repulsion arising from charges on the protein and hydrophobic attraction, originating from the exposure of hydrophobic residues by thermal denaturation [14–16]. Other forces, such as hydration and van der Waals interactions, while less prominent, can also play a critical role in protein gelation. The delicate interplay of these interactions can be tuned by varying suitable physicochemical parameters and adding certain additives to gain control over the gelation mechanism and properties [12,17–19]. It has been recently shown that the heat-induced unfolding and gelation of protein can be restricted using multivalent counterions such as Zr^{4+} [20]. The emergence of strong hydration interaction due to increased surface dipoles from the excess condensation of Zr^{4+} ions is believed to suppress the exposure of the hydrophobic patches of protein and therefore prevent protein gelation [20]. The hydrogelation of β-hairpin peptides has been tuned by hydrophobic amino acid substitutions, where the peptide self-assembly, hydrogelation rates, and mechanical stiffness of gel are found to be increasing with hydrophobicity [21]. There are other suitable additives (e.g., polysaccharides, polyelectrolytes, amphiphiles, etc.) which can interact with proteins via either hydrophobic or electrostatic or both interactions and hence open pathways to selectively direct protein gelation [22–25]. In this regard, the choice of the amphiphiles is also motivated by its practical implications, where the protein-amphiphile complexes are extensively utilized in drug delivery applications, cosmetics, and the food industry [26–29].

Surfactants which are amphiphiles are known to interact strongly (especially the ionic surfactants) with protein due to their common amphiphilic and charge nature [26,28]. The charged head group of ionic surfactants interacts with the oppositely charged patches of the protein chain, whereas hydrophobic (alkyl) tails of surfactants bind to the hydrophobic patches of proteins [29]. Recently, MD simulations have been used to show that both of these interactions (hydrophobic and electrostatic) are equally important in forming protein-surfactant complexes [30]. However, despite the possibility of a strong role of hydrophobic interaction, nonionic surfactants

*sugam@barc.gov.in
†vkaswal@barc.gov.in

do not or weakly interact with the proteins, but their self-assembly with ionic surfactants plays a crucial role in protein unfolding and refolding [31–33]. The ability of surfactants to drive the interplay of hydrophobic and electrostatic interactions in protein solutions is expected to influence protein gelation in terms of sol-gel transition, gelation temperature, and gel structure [22,23,34–37]. It is, therefore, interesting to understand the effect of surfactants on heat-induced protein gelation.

Herein, we propose a pathway to control protein gelation at elevated temperatures by tuning these (hydrophobic and electrostatic) interactions in presence of surfactants. We dictate the bovine serum albumin (BSA) protein gelation via introducing anionic [sodium dodecyl sulfate (SDS)] and nonionic [decaoxyethylene $n-$dodecylether ($C_{12}E_{10}$)] surfactants in the system [26,29,36–38]. The presence of SDS prevents protein gelation even up to significantly higher temperatures, whereas $C_{12}E_{10}$ supports protein gelation [25,37]. Further, the SDS-induced resistance of the protein against gelation is suppressed by adding $C_{12}E_{10}$ in the system. The observations are counterintuitive, as the ionic surfactant is expected to act as a denaturant and support protein gelation. On the other hand, the nonionic surfactant is believed to remain neutral and not contribute in the gelation process (discussed later in the paper). Optical transmission and rheology measurements have been used to establish gel formation, while small-angle neutron scattering (SANS) and dynamic light scattering (DLS) have been employed to investigate the evolution of interactions and structures and understand the mechanism responsible for these intriguing observations.

II. EXPERIMENTAL

A. Materials and sample preparation

BSA protein and surfactants [anionic SDS and nonionic decaoxyethylene $n-$dodecylether ($C_{12}E_{10}$)] were purchased from Sigma-Aldrich. Samples were prepared by dissolving the weighted amount of the components in 20 mM pH 5 acetate buffer in D_2O for SANS and in H_2O for other measurements. Due to the low solute concentrations, these solutions do not show any significant changes in density as compared to water. It may be noted that the pH 5 is close to the isoelectric point ($pI \sim 4.7$) of the BSA, where the charge on the protein is negative but sufficiently low to suppress the electrostatic repulsion and facilitate the gelation of the pristine BSA at gelation temperature. The use of D_2O as solvent in SANS is essential to get sufficient contrast for hydrogenous scatterers (e.g., protein and surfactants) and to reduce the hydrogen-generated incoherent background. All the samples were freshly prepared and equilibrated for sufficient time to eliminate any bubble formation. The measurements were made within 12 h of sample preparation, and no aging effects were observed within this time frame. The protein gels are obtained by heating the samples till gelation temperature. All the samples were equilibrated for about 30 min at a given temperature. This procedure was repeated multiple times to ensure the reproducibility of the results and to get the average value of the gelation temperatures (within error bars).

B. Measurements

Dynamic light scattering and optical transmission. The DLS and optical measurements were carried out using a nanoparticle size analyzer SZ-100 (Horiba, Japan). The instrument contains a 10 mW diode-pumped solid-state laser with a wavelength of 532 nm. The autocorrelation functions (ACFs) were measured at a back-scattering angle 173° (wave vector transfer $Q \sim 0.0023$ Å^{-1}) using a photomultiplier tube detector. The measurements were repeated five times to ensure consistency and capture errors in the results. The backscattering angle was used for the measurements for minimizing multiple scattering from samples (particularly at near gelation temperature) by reducing the path length of the laser light within the samples. The transmissions of the samples were measured by the same instrument, utilizing the transmission monitor at a 0° scattering angle.

Small-angle neutron scattering (SANS). The SANS measurements were performed at the SANS-I facility at the Dhruva reactor, Bhabha Atomic Research Centre, Mumbai, India [39]. A monochromatized neutron beam of mean wavelength ($\lambda \sim 5.2$ Å) with a spread of $\Delta\lambda/\lambda \sim 15\%$ is made incident on the sample. The angular distribution of neutrons scattered by the sample is recorded using a number of 1 m long one-dimensional ^{3}He position-sensitive detectors placed in crossed-geometry. The instrument covers a wave vector transfer [$Q = (4\pi \sin\theta)/\lambda$; 2θ is the scattering angle] range of 0.01–0.3 Å^{-1}. The data were corrected for transmission, empty cell contribution, and backgrounds and normalized to an absolute scale using standard protocols [39,40].

Rheology. Rheological measurements of the protein gels were carried out with an Anton Paar Physica MCR101 rheometer using parallel plate geometry and Peltier temperature control system. The samples (4 wt % BSA, 4 wt % BSA + 40 mM $C_{12}E_{10}$, and 4 wt % BSA + 6 mM SDS + 40 mM $C_{12}E_{10}$) were heated to a temperature (80° C), above T_G, to gel the protein prior to the measurements. Samples were then cooled down to room temperature for rheology measurements in ambient conditions. These gels were scooped out with a spatula and were placed between the two parallel plates before the application of shear by the rotating upper plate. The rates of oscillatory shear were varied from 1 to 1000 sec^{-1}.

Viscometry. Sample 4 wt % BSA + 6 mM SDS does not form gel, even after heating at 80° C for longer times (discussed later in Results and Discussion). Therefore, instead of rheology [storage (G') and loss (G'') moduli], the viscosity measurements were carried out for this sample (4 wt % BSA + 6 mM SDS), using a Cannon Ubbelohde calibrated viscometer with viscometer constant value of 0.004065 centistokes sec^{-1}. The temperature of the sample in the viscometer was fixed using a water bath within ±2° C for a given temperature. Multiple measurements were carried at a temperature to get an average flow time (within ±5 sec). The kinematic viscosity of the solutions in centistokes is obtained by multiplying flow times by the viscometer constant. Absolute viscosities (in centipoise) were then calculated by multiplying kinematic viscosity values with the density of water (taken as 1 g/cc).

C. Data analysis

1. Dynamic light scattering (DLS) analysis

In DLS one measures fluctuation in the intensity of scattered light in terms of autocorrelation functions. The normalized electric field autocorrelation function of the scattered light for monodispersed system is written as [41,42]

$$g^1(\tau) = e^{-\Gamma\tau}, \tag{1}$$

where $\Gamma(= DQ^2)$ is the decay constant, which further depends on translational diffusion coefficient (D) and magnitude of wave vector transfer (scattering vector) Q. The electric field autocorrelation function $[g^1(\tau)]$ is related to normalized intensity autocorrelation function $[g^2(\tau)]$ by the following Siegert relation:

$$g^2(\tau) = 1 + \beta|g^1(\tau)|^2, \tag{2}$$

where β is the spatial coherence factor, decided by instrument optics, and defines the resolution of the instrument.

For polydispersed system, the $g^1(\tau)$ can be convoluted with the distribution of decay constants $[G(\Gamma)]$, using the following Laplace transformation:

$$g^1(\tau) = \int_0^\infty G(\Gamma)\exp(-\Gamma\tau)\,d\Gamma. \tag{3}$$

In the case of narrow monomodal distribution, the cumulant analysis is usually used, and in this method, $g^1(\tau)$ is given by [41]

$$g^1(\tau) = \exp\left(-\bar{\Gamma}\tau + \frac{\mu_2\tau^2}{2}\right), \tag{4}$$

where $\bar{\Gamma}$ denotes the mean decay constant and μ_2 represents the variance. The diffusion coefficient of the system is calculated from the decay constant of the autocorrelation function.

The Stokes-Einstein relation is then used to obtain the mean hydrodynamic size (d_h) of the particles and scatterers

$$d_h = \frac{k_BT}{3\pi\eta D}, \tag{5}$$

where T is absolute temperature, k_B is the Boltzmann's constant, and η is the viscosity of the solvent. The polydispersity index is then obtained as the ratio of variance to the square of the mean size.

It may be noted that d_h is also influenced by the interactions present in the system, where the attractive interaction causes an apparent increase in the effective hydrodynamic size, while repulsion leads to a decrease in d_h [41,42].

2. Small-angle neutron scattering (SANS) analysis

SANS analysis measures the differential scattering cross section per unit volume ($d\Sigma/d\Omega$) as a function of Q. For a system of monodisperse interacting particles in a medium (e.g., protein molecules dispersed in D_2O), $d\Sigma/d\Omega$ can be given as [43,44]

$$\left(\frac{d\Sigma}{d\Omega}\right)(Q) = nP(Q)S(Q) + B, \tag{6}$$

where n is the number density of scatterers, $P(Q)$ is the intraparticle structure factor (square of form factor), and $S(Q)$ denotes interparticle structure factor. B is a constant term representing the incoherent background, mainly originating from hydrogen present in the sample.

Intraparticle structure factor $P(Q)$ is governed by shape and size of the particle. For a spherical particle of radius R and volume V, $P(Q)$ is given by [44]

$$P(Q) = V^2(\rho_p - \rho_s)^2\left\{\frac{3[\sin(QR) - QR\cos(QR)]}{(QR)^3}\right\}^2, \tag{7}$$

where ρ_p and ρ_s represent the scattering-length densities of the particles and solvent, respectively.

The $P(Q)$ for ellipsoidal particle can be expressed as [44]

$$P(Q) = V^2(\rho_p - \rho_s)^2\int_0^1 [F(Q,\mu)]^2 d\mu, \tag{8}$$

where $F(Q,x) = \frac{3(\sin x - x\cos x)}{x^3}$ in this $x = Q[a^2\mu^2 + b^2(1-\mu^2)]^{\frac{1}{2}}$

The parameters a and b denote the semiaxes for ellipsoid shape, and μ is the cosine of the angle between the direction of major axis and scattering vector Q. The BSA protein is usually described by an oblate ($b = c > a$) ellipsoidal shape [19,20]. The nonionic $C_{12}E_{10}$ micelles have been modeled using $P(Q)$, calculated for a spherical core attached with a Gaussian chain model, as described in Ref. [45].

The $S(Q)$ is governed by the interactions between particles by the Ornstein-Zernike relation along with a proper closure relation. Most of the physical systems are governed by different short- or long-range attractive and repulsive interactions, present in the system. Therefore, in this study, the $S(Q)$ has been calculated by modeling the interaction between scatterers (proteins) by a two-Yukawa (2Y) potential with the mean spherical approximation [46–48]. The 2Y potential (in units of k_BT) comprises two exponential terms and can be expressed as [46–48]

$$\frac{V(r)}{k_BT} = \infty\,(0 < r < \sigma) = K_1\frac{\exp[-Z_1(r/\sigma - 1)]}{r/\sigma} - K_2\frac{\exp[-Z_2(r/\sigma - 1)]}{r/\sigma}\,(r > \sigma) \tag{9}$$

where r and σ denote interparticle distance and hard sphere diameter of the particle, respectively. The repulsive (first term) and attractive (second term) parts of the total interaction potential can be separately modeled in the 2Y potential. Hence, use of 2Y potential enables the determination of magnitude and range of respective parts of the potential without any predefined assumption or limitations. There are four dimensionless parameters (K_1, K_2, Z_1, and Z_2), where K_1 and K_2 are proportional to the strength while Z_1 and Z_2 are inversely proportional to range of the repulsive and attractive parts of the interaction, respectively. It may be added here that the 2Y potential can take account of the DLVO (Derjaguin-Landau-Verwey-Overbeek) potential, where the van der Waals attraction can be simulated by a short-range Yukawa potential and the repulsive part can be compared with the screened Coulomb potential for charged proteins as per Debye-Hückel (DH) theory [47]. Moreover, the potential can also take account of other non-DLVO attraction or repulsion by simply changing K_i ($i = 1, 2$) and Z_i [46–48]. For a sufficiently dilute

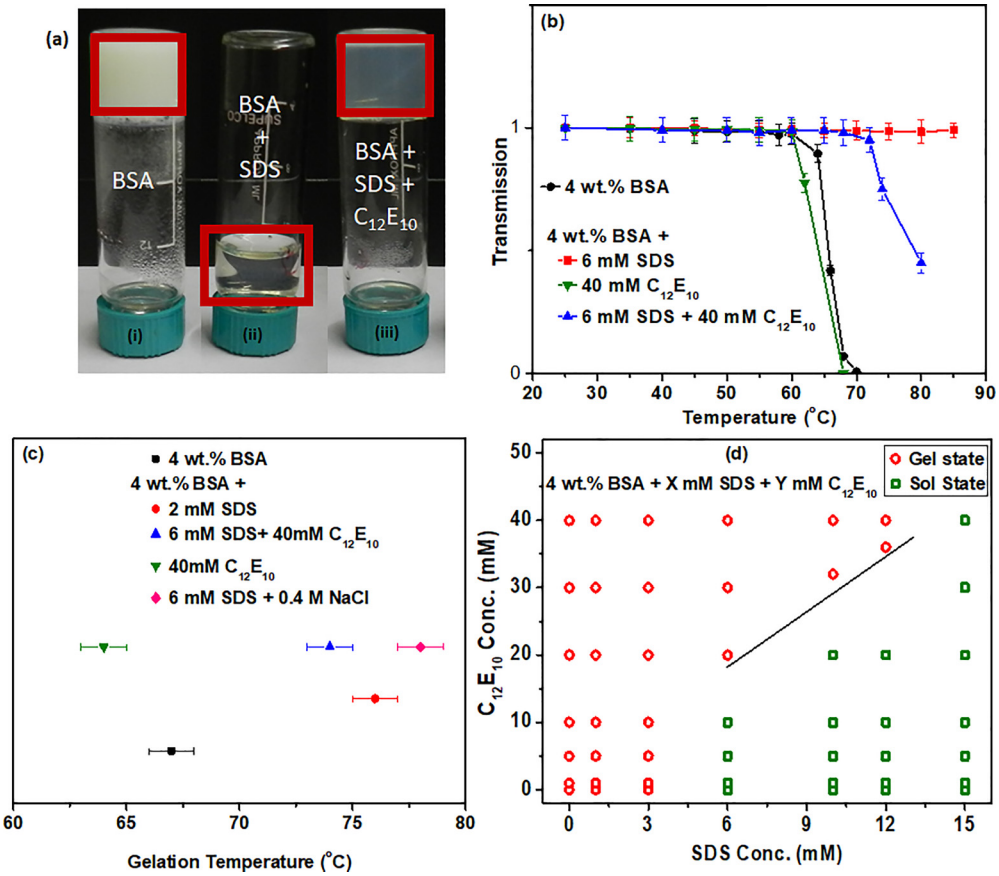

FIG. 1. (a) Physical states of 4 wt % BSA, 4 wt % BSA + 6 mM SDS, and 4 wt % BSA + 6 mM SDS + 40 mM $C_{12}E_{10}$ samples heated at 80° C, (b) optical transmission of 4 wt % BSA in the presence and absence of surfactants as a function of temperature, (c) gelation temperature of protein samples as obtained from optical transmission (the points are shifted vertically to avoid overlap between their error bars and to ensure visual clarity), and (d) phase diagram for gelation of 4 wt % BSA in the presence of SDS and/or $C_{12}E_{10}$ (circles and squares denote gel formation and solution states of samples at 80° C, respectively). The black line in Fig. 1(d) represents a phase boundary, suggesting a requirement of at least three times $C_{12}E_{10}$ concentration compared to that of the SDS to achieve gelation in the BSA + SDS + $C_{12}E_{10}$ samples.

system (e.g., nonionic $C_{12}E_{10}$ micelles at low concentration), $S(Q)$ may be approximated to unity.

Scattering cross sections for a system consisting of two independent entities can be given by the sum of scattering from individual components. For example, in the case of BSA protein coexisting with mixed $C_{12}E_{10}$ + SDS micelles (discussed later), the scattering cross section can be given by [49]

$$\left(\frac{d\Sigma}{d\Omega}\right)(Q) = \left(\frac{d\Sigma}{d\Omega}\right)_P(Q) + \left(\frac{d\Sigma}{d\Omega}\right)_m(Q), \qquad (10)$$

where subscripts p and m represent scattering cross sections from protein and micelles, respectively. $P(Q)$ and $S(Q)$ can be accordingly used for the respective components.

The data analysis has been carried out by fitting the experimental data with the scattering calculated for different suitable theoretical models, and the parameters were optimized by employing nonlinear least square fitting methods. Throughout the data analysis, corrections were also made for instrumental smearing [44]. The modeled scattering profiles were smeared by the appropriate resolution function to compare with the measured data.

III. RESULTS AND DISCUSSION

Figure 1 shows the macroscopic behavior of the 4 wt % BSA solution in the absence and presence of surfactants as a function of temperature. The photographs of the tube inversion test [Fig. 1(a)] show that the heating of 4 wt % (anionic) BSA above gelation temperature transforms the solution into gel [Fig. 1(a)-(i)]. The heating of the protein results in protein denaturation by breaking the hydrogen and disulfide bonds, leading to the exposure of internally directed hydrophobic sites of the protein [18]. The instability of these sites in an aqueous environment gives rise to net hydrophobic attraction among protein molecules, finally causing the system to undergo gelation. In general, the addition of chemical denaturants is known to support heat-driven protein aggregation and gelation [22,36,50–52]. For example, gelation temperature is observed to be reduced significantly for BSA protein solutions prepared at lower pH, where the protein is known to exist in an extended conformation [50]. Similarly, the addition of tetramethylurea, a chemical denaturant, is reported promoting solvent-induced gelation of lysozyme protein [51]. Further, the reduction in the gelation time for BSA protein has been reported on the addition of cetyltrimethylammonium bromide surfactant [52]. Referring to the above cases, the addition of

SDS, a protein denaturant, is expected to support BSA gelation. However, contrary to this, the addition of 6 mM SDS in the BSA solution prevents protein gelation [Fig. 1(a)-(ii)] even after heating the sample at a higher temperature ($\sim 85^\circ$ C) and for a longer time (~ 2 h) [23,25,53]. On the other hand, the nonionic surfactant ($C_{12}E_{10}$), which is known to either weakly or not interact with protein [31,32], supports the protein gelation by reducing T_G [Fig. S1 in the Supplemental Material (SM) [54] and Fig. 1(c), discussed later]. Interestingly, the BSA+SDS sample undergoes heat-driven gelation on the addition of 40 mM $C_{12}E_{10}$, suggesting that the protecting effect of SDS against gelation can be suppressed by incorporating nonionic surfactant $C_{12}E_{10}$ in the system [Fig. 1(a)-(iii)].

The phase behavior of BSA with and without surfactants have been evaluated by measuring the optical transmission of the samples as a function of temperature [Fig. 1(b)] [19]. The transmissions plotted in Fig. 1(b) are normalized to the transmission of the 4 wt % BSA solution, measured at 25° C. The formation of the larger or network structure in the sample gives rise to a decrease in the optical transmission [19]. The transmission of the 4 wt % BSA sample shows an abrupt decrease at around 65° C and becomes almost zero for temperatures above 68° C. However, no significant decrease in the transmission of BSA+SDS solution is seen, suggesting that the system does not undergo gelation, even at higher temperatures. The same system shows a decrease in the transmission on the addition of 40 mM $C_{12}E_{10}$, further suggesting that the suppression of gelation can be reversed by incorporation of a nonionic surfactant. The BSA (4 wt %) solution also undergoes gelation in the presence of $C_{12}E_{10}$ alone (Fig. S1 in SM [54]), indicating that (1) the behavior of the protein towards gelation is different in the presence of ionic and nonionic surfactants and (2) the mutual interactions of the two surfactants with each other as well as with the protein are playing a critical role in deciding the formation of gel [26,28,31]. The measured optical transmissions are also used to determine the gelation temperature of the samples, as depicted in Fig. 1(c). The gelation of the BSA is observed to be taking place at temperature about 67° C, which decreases to a lower temperature ($\sim 64^\circ$ C) in the presence of $C_{12}E_{10}$. The gelation temperature of the BSA + SDS + $C_{12}E_{10}$ sample increases compared to that for pristine BSA and BSA + $C_{12}E_{10}$ solutions. It should be noted that gelation of the BSA+SDS sample can also be achieved by adding a sufficient amount of salt, apart from $C_{12}E_{10}$ surfactant. However, the gelation temperature of sample (4 wt % BSA + 6 mM SDS + 0.4 M NaCl) is observed to be maximum.

Figure 1(d) depicts the complete phase diagram of gelation of 4 wt % BSA in the presence of SDS and $C_{12}E_{10}$. As may be noted, at low concentrations of SDS ($\leqslant 3$ mM) the BSA + SDS system undergoes gelation, and the gelation temperature [e.g., for 4 wt % BSA + 2 mM SDS sample, $T_G \sim 76^\circ$ C; Fig. 1(c)] is noted to be significantly higher than that of the pure BSA solution. As the SDS concentration increases, the protein gelation is restricted, and the solution states of the BSA+SDS system do not undergo gelation even at much higher temperatures for SDS concentrations more than a critical concentration $C_{SDS} > 5$ mM. At all concentrations of $C_{12}E_{10}$, the BSA + $C_{12}E_{10}$ system undergoes gelation, where the gelation temperature remains less than that of the pure BSA solution. The SDS-induced suppression of the BSA gelation can be reversed by adding a minimum amount of the $C_{12}E_{10}$. A linear line along the phase boundary for SDS concentrations more than C_{SDS} suggests a requirement of at least three times $C_{12}E_{10}$ concentration compared to that of the SDS, to achieve gelation in the BSA + SDS + $C_{12}E_{10}$ samples.

The gel characteristics of all the gel samples were measured by carrying out frequency sweep tests in rheology measurements. All the samples (pure BSA and in the presence of SDS/$C_{12}E_{10}$) were heated at 80° C, prior to the measurements. The measured storage (G') and loss (G'') moduli as a function of oscillatory shear frequency for the gel samples are shown in Fig. 2(a). For all the gel samples [4 wt % BSA, 4 wt % BSA + 40 mM $C_{12}E_{10}$, and 4 wt % BSA + 6 mM SDS + 40 mM $C_{12}E_{10}$], storage or elastic modulus (G') is higher than loss or viscous modulus (G''), confirming the typical signatures of gel formation [9,50,55]. As can be observed, the variation of G' does not show a significant frequency dependence, and the slope of the profile remains more or less zero for all the gel samples, further exhibiting the hard nature of the formed gels. G' and G'' for both the 4 wt % BSA and 4 wt % BSA + 6 mM SDS + 40 mM $C_{12}E_{10}$ samples are observed to be approximately the same in the entire frequency range, suggesting that the gel formed by addition of 40 mM $C_{12}E_{10}$ in BSA+SDS sample has almost similar rheological behavior to that of pure BSA gel. However, G' is noted to be higher for the 4 wt % BSA + 40 mM $C_{12}E_{10}$ sample, compared to the other two samples, suggesting the formation of gel with larger strength in this case. The higher storage modulus and lower gelation temperature of the 4 wt % BSA + 40 mM $C_{12}E_{10}$ sample indicate that the presence of $C_{12}E_{10}$ supports the BSA gel formation. For the sample 4 wt % BSA + 6 mM SDS which has not been converted into gel, viscosity measurements have been carried out [Fig. 2(b)], and the measured viscosity does not show any significant change as a function of the temperature, further supporting the prevention of protein gel in the presence of SDS.

In order to understand these interesting observations in gelation behavior, the structural and interactional evolution in BSA samples, with and without surfactants, as a function of temperature has been probed by DLS and SANS. The DLS and SANS measurements of all the samples were carried out at temperatures below the gelation temperature of the respective sample, where the sample remains in the fluid form. Fig. 3(a) shows the intensity autocorrelation functions (ACFs) of 4 wt % BSA with increasing temperature, as measured by DLS. The initial rise in temperature up to 50° C, leads to a slight shift of ACFs towards shorter relaxation times. This shift in the ACFs may be attributed to the faster diffusion in the system with increasing temperature, as cumulant analysis of DLS data does not show any changes in hydrodynamic sizes [Fig. 3(b)]. However, a further rise in the temperature ($> 50^\circ$ C) shifts the ACFs towards longer relaxation times, suggesting either the formation of larger structures or the evolution of attraction in the system. For temperatures 50° C $< T < 60^\circ$ C, there is shifting of ACFs towards longer relaxation times but almost no change in the transmission [Fig. 1(b)]; therefore slower decay rate may be attributed to the evolution of attractive interaction

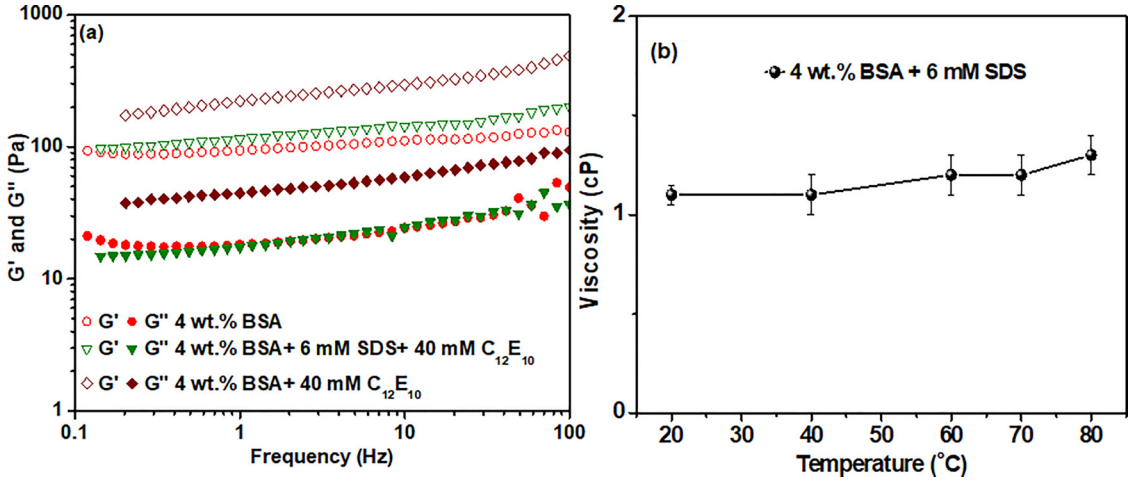

FIG. 2. (a) Storage (G') and loss (G'') moduli vs oscillatory shear frequency plots of the gel samples and (b) the change in the viscosity of the 4 wt % BSA + 6 mM SDS as a function of temperature.

in the system. The calculated effective hydrodynamic size also shows only a slight increase [Fig. 3(b)] [41,56]. For temperatures ($> 62^\circ$ C), where transmission of 4 wt % BSA decreases substantially, a significant shift in ACFs towards longer decay time is observed and attributed to the denaturation of protein and formation of the larger aggregates, which forms an interprotein matrix at gelation temperature [56]. It should be noted that the polydispersity index also increases as

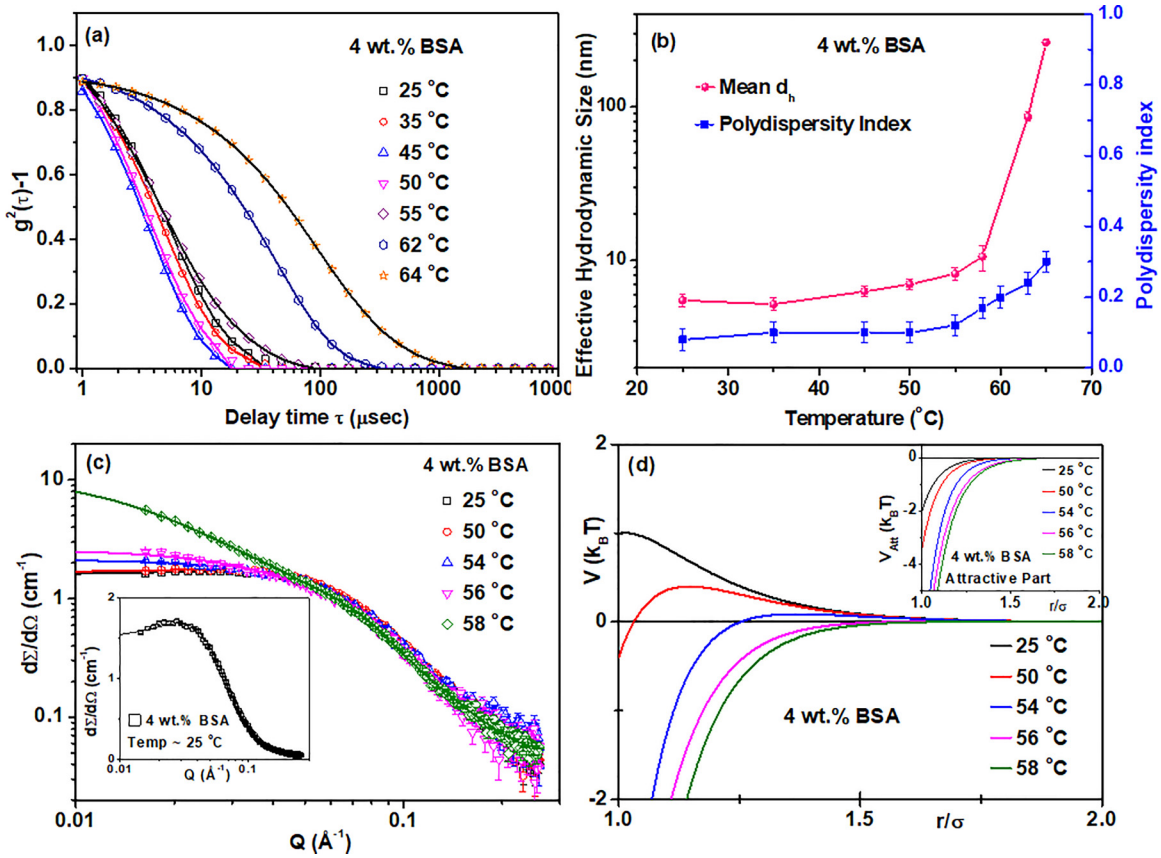

FIG. 3. (a) ACFs of 4 wt % BSA solution as measured by DLS with increasing temperature, (b) variation in the calculated effective mean hydrodynamic size (d_h) and polydispersity index, with increasing temperature, as obtained from the DLS data (a), and (c) SANS data of the 4 wt % BSA system with increasing temperature. The black lines in Fig. 3(c) represent fits to Eq. (6), where $P(Q)$ and $S(Q)$ are determined by Eqs. (8) and (9). The data of pure BSA solution show a broad correlation peak at $Q_p \sim 0.028$ Å^{-1} [inset of Fig. 3(c)]. (d) Fitted total interaction potentials between protein molecules with rise in temperature. Inset of (d) shows attractive part of the total potentials depicting the enhancement in the attraction among protein molecules on increasing solution temperature.

TABLE I. Fitted parameters for the 4 wt % BSA with increasing temperature. The data are analyzed considering unfolded protein undergoing attractive interaction. The form factor of oblate ellipsoidal shape and structure factor calculated for 2Y potential were used to fit the data. At 25° C, the parameters for the attraction were kept fixed, equivalent to van der Waals attraction, while those corresponding to repulsion were allowed to fit. For higher temperatures, the parameters of repulsion were kept fixed equal to that obtained at 25° C, while those of attraction were fitted to account for additional hydrophobic attraction.

Temperature (°C)	Semimajor axis $b = c$ (nm)	Semiminor axis a (nm)	K_1 (k_BT)	Z_1	K_2 (k_BT)	Z_2
25	4.2 ± 0.3	1.4 ± 0.1	3.0 ± 0.3	6.0 ± 0.5	2.0 ± 0.2	10.0 ± 0.6
50	4.2 ± 0.3	1.4 ± 0.1	3.0 ± 0.3	6.0 ± 0.5	3.4 ± 0.2	10.0 ± 0.6
54	4.2 ± 0.3	1.4 ± 0.1	3.0 ± 0.3	6.0 ± 0.5	8.2 ± 0.2	10.0 ± 0.6
56	4.4 ± 0.3	1.4 ± 0.1	3.0 ± 0.3	6.0 ± 0.5	9.0 ± 0.2	8.0 ± 0.6
58	4.8 ± 0.3	1.4 ± 0.1	3.0 ± 0.3	6.0 ± 0.5	11.0 ± 0.5	8.0 ± 0.6

the gelation temperature approaches, mostly because of the statistical nature of temperature-induced protein unfolding, thereby, aggregation and gelation process [Fig. 3(b)].

The evolution of structure and interaction in the system can be obtained by modeling inter- and intraparticle structure factors in the SANS data [43,47]. SANS data of the 4 wt % BSA as a function of temperature are shown in Fig. 3(c). In the SANS data [$d\Sigma/d\Omega(Q)$ vs Q] of pristine 4 wt % BSA at 25° C, a broad correlation peak ($Q_p \sim 0.028$ Å^{-1}) can be observed [inset of Fig. 3(c)]. Such a peak usually appears at $Q \sim 2\pi/d$ (where d is the interparticle separation) and indicates the presence of interacting scatterers (BSA molecules). The data are analyzed using a form factor of oblate ellipsoidal and a structure factor calculated using 2-Yukawa potential. The BSA protein is found to have a semimajor ($b = c$) axis 4.2 nm and semiminor axis (a) 1.4 nm. These dimensions are consistent with those determined by analyzing the SANS data of dilute (1 wt %) BSA solution at 25° C using oblate ellipsoidal form factor as well as the proper crystal structure of the BSA monomer obtained from the Protein Data Bank (PDB file code 4F5T) (Fig. S2 and Table ST1 in SM [54]) [20,47,56]. For pure BSA at 25° C, in the fitted total interaction potential, the repulsive part corresponds to the screened Coulomb potential, whereas the attractive part is modeled with parameters equivalent to that for van der Waals attraction [20,46,47].

The SANS data [Fig. 3(c)] of pure BSA do not show significant changes for temperatures less than 50° C, consistent with almost no change in the measured hydrodynamic size. However, for temperatures $\geqslant$ 50° C, the correlation peak disappears, and an increase in the scattering intensity in the low-Q region is observed [Fig. 3(c)], which could be because of the emergence of attraction between proteins in accordance with DLS and transmission measurements. Moreover, the form-factor-governed scattering, appearing mainly in the Q range > 0.05 Å^{-1}, remains unchanged in the temperature range of the measurements, suggesting minor changes (if any) in the structural parameters. The data at temperatures above 50° C are also fitted by considering the form factor of the oblate ellipsoidal and interparticle structure factor as calculated for 2Y potential, and the fitted parameters are listed in Table I. To fit the data at higher temperatures ($\geqslant$ 50° C), the parameters of repulsive interaction were kept fixed, equivalent to that obtained from SANS data at 25° C, while those of the attraction were allowed to float. The structural dimensions are found to be slightly larger than those of native structure at temperatures $\geqslant$ 56° C (Table I), suggesting that the significant conformational changes in protein must be occurring at temperatures close to T_G [20]. A systematic transition from a repulsive to an attractive system can be seen with increasing temperature, primarily due to the contribution of hydrophobic interaction, which finally drives protein gelation. Further, the range of attraction slightly increases with increasing temperature from 54 to 56° C. This could be because the temperature-driven hydrophobic attraction is evolving at these temperatures. The first increase in the structural dimension also occurs in this temperature range, suggesting that the protein starts unfolding as the temperature increases from 54 to 56° C. However, the major impact of the rise in temperature appears on the strength of the attraction.

The DLS and SANS data of the 4 wt % BSA sample in the presence of 6 mM SDS are shown in Fig. 4. On increasing the temperature, the ACFs of the 4 wt % BSA + 6 mM SDS system show a shift only towards shorter decay time and no shift towards longer relaxation times, contrary to the variation observed in ACFs for pristine BSA solution. The shift towards shorter decay time can be understood due to the rise in temperature and corresponding changes in the diffusion of protein and viscosity of the medium. This is also consistent with the analysis of the data, which does not show any significant increase in the effective mean hydrodynamic size of the 4 wt % BSA + 6 mM SDS sample with increasing temperature, confirming the suppression of the gelation [Fig. 4(b)].

The suppression of gelation in 4 wt % BSA + 6 mM SDS system is also evident from SANS data [Fig. 4(c)]. The scattering profile of the 4 wt % BSA + 6 mM SDS sample shows lower scattering in the low-Q region compared to that of pristine 4 wt % BSA [20]. This implies that BSA has more repulsive interaction in the presence of SDS. The protein interaction with surfactants proceeds mainly via the following three steps: specific binding, cooperative binding, and saturation, based on the relative concentration of two components [26,28,29,31,32]. At low surfactant concentrations, individual surfactant monomers bind to specific binding sites of the protein (specific binding) in a noncooperative manner, retaining the folded structure of the protein. During this process, the charged head group of surfactant binds to the oppositely charged side chains, while binding of the alkyl chains occurs to nearby hydrophobic patches. The cooperative binding of surfactant with protein takes place at relatively higher surfactant concentrations via the formation of micelle-like clusters along the unfolded polypeptide chain. Further

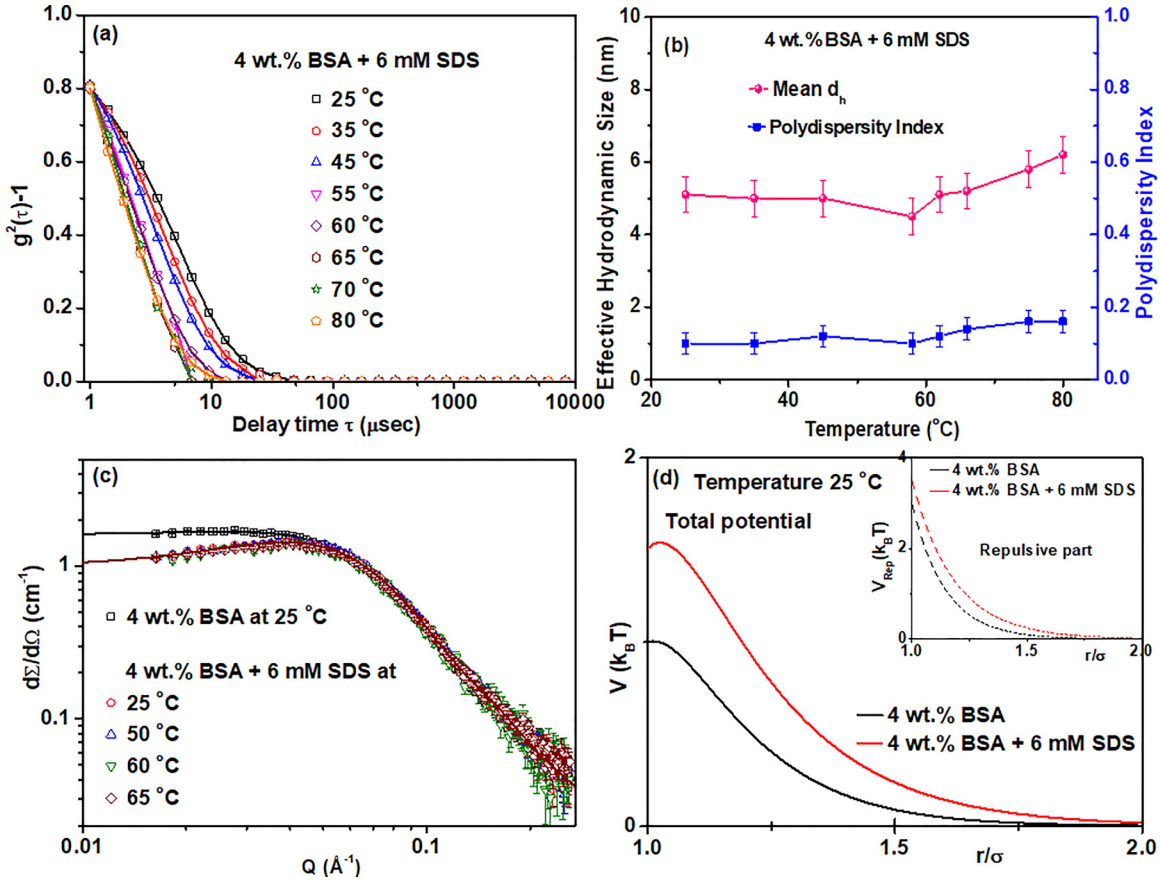

FIG. 4. (a) ACFs of 4 wt % BSA+ 6 mM SDS solution as measured by DLS with increasing temperature, (b) variation in the effective mean hydrodynamic size (d_h) and polydispersity index with increasing temperature as calculated using the DLS data (a), (c) SANS data of the 4 wt % BSA at 25° C (black square) and 4 wt % BSA+6 mM SDS system with increasing temperature, and (d) comparison of fitted total interaction potentials between protein molecules at 25° C, in the absence and presence of SDS. Inset of (d) shows the comparison of the repulsion experienced by protein molecules in the absence and presence of SDS at 25° C.

increase in surfactant concentration enhances the cooperative binding until the saturation region is achieved, where the excess surfactant does not bind to protein and coexists with the protein-surfactant complexes. The exact boundaries of these three regimes of the SDS concentration depend on effective interaction between the two components, which is further decided by several physicochemical factors, such as pH or ionic strength of the solution, protein concentration, amount and nature of charge on protein, etc.

In the present study, the concentration of SDS (6 mM, which is less than CMC of SDS $\sim$ 8 mM) is in the specific or noncooperative binding region as evident from SANS or DLS data, where no unfolding of BSA (4 wt %) is observed at 6 mM SDS at 25° C [31,38]. This has further been confirmed by performing indirect Fourier transformation of SANS data, where the absence of a second peak in pair distance distribution function $p(r)$ of 4 wt % BSA + 6 mM SDS also supports the folded structure of BSA (Fig. S3 in SM [54]) [32,43]. At 6 mM concentration, SDS though unable to unfold the protein, gives rise to enhanced charge-charge repulsion between these protein-surfactant complexes, as reflected in the SANS data [Fig. 4(c)], via specific binding of surfactant to oppositely charged patches of BSA. The SANS data of 4 wt % BSA + 6 mM SDS has also been modeled using an oblate ellipsoidal shape, including the interaction via 2Y potential. The fitted parameters are provided in Table II. The total interaction potential of the BSA+SDS system is found to be more repulsive than that of the pristine BSA at 25° C [Fig. 4(d)].

The increase in temperature of the 4 wt % BSA + 6 mM SDS system does not significantly alter the structural and interactional parameters, evidencing the suppression of the protein gelation (Table II). The data analysis shows that this suppression can be largely attributed to the increased electrostatic repulsion between protein-surfactant complexes [Fig. 4(d)]. This is also validated by attaining the gelation of the BSA-SDS system on the addition of salt (0.4 M NaCl), where the salt ions screen the electrostatic repulsion between BSA-SDS complexes (Fig. S4 in SM [54]). Moreover, the low SDS concentration ($\leqslant$ 2 mM) is also not able to restrict the gelation of the BSA+SDS system, probably because the SDS amount is not adequate to cause sufficient electrostatic repulsion between complexes (Fig. S5 in SM [54]). Similar stabilization of *Humicola insolens* cutinase (HiC) by high concentration of SDS against thermal aggregation has also been suggested because of electrostatic repulsion between increasingly negatively charged HiC-SDS complexes [53]. However, molecular dynamics simulations have shown that SDS also

TABLE II. Fitted parameters for the 4 wt % BSA + 6 mM SDS system with increasing temperature. The parameters for attraction were kept fixed, corresponding to those obtained for pure BSA at 25° C, as the SANS data did not show any signature of evolution of attraction.

Temperature (°C)	Semimajor axis $b = c$ (nm)	Semiminor axis a (nm)	K_1 (k_BT)	Z_1	K_2 (k_BT)	Z_2
25	4.2 ± 0.3	1.4 ± 0.1	3.5 ± 0.2	4.5 ± 0.2	2.0 ± 0.2	10.0 ± 0.6
50	4.2 ± 0.3	1.4 ± 0.1	3.6 ± 0.3	4.5 ± 0.2	2.0 ± 0.2	10.0 ± 0.6
60	4.2 ± 0.3	1.4 ± 0.1	3.8 ± 0.3	5.0 ± 0.5	2.0 ± 0.2	10.0 ± 0.6
65	4.2 ± 0.3	1.4 ± 0.1	3.7 ± 0.3	5.5 ± 0.5	2.0 ± 0.2	10.0 ± 0.6

reduces the water density near BSA by forming more BSA-SDS hydrogen bonds than BSA-water bonds, thereby reducing the impact of hydrophobic attraction [23]. Therefore, SDS-driven prevention of protein gelation at higher temperatures may be arising because of modifications, in both electrostatic as well as hydrophobic interactions.

Such SDS-induced resistance of protein against gelation can be reversed by introducing a nonionic surfactant $C_{12}E_{10}$ in the system, as seen in Fig. 1. The nonionic $C_{12}E_{10}$ surfactant is known to remain largely noninteractive with the protein, despite the possibility of altering the hydrophobic interaction [29,57]. It, therefore, does not have the possibility of causing changes in protein conformation. Fig. 5(a) shows the DLS data of the 4 wt % BSA + 10 mM + 40 mM $C_{12}E_{10}$ system with increasing temperature. The effective mean hydrodynamic size of the 4 wt % BSA + 10 mM + 40 mM $C_{12}E_{10}$ system is observed to be around 8 nm [Fig. 5(b)], which is roughly similar to that of pure protein. It should be mentioned here that the $C_{12}E_{10}$ micellar size is approximately similar to that of the effective size of the protein. Therefore, the hydrodynamic size obtained in the DLS cannot distinguish between these two entities. As observed for the pure 4 wt % BSA solution, the autocorrelation functions in this case also show a shift towards lower decay time for temperatures $\leqslant 55°$ C. This can be simply attributed to the temperature-driven faster diffusion, as no significant change in the effective hydrodynamic size has been observed. However, a further increase in the temperature leads to the shifting of the ACFs towards larger

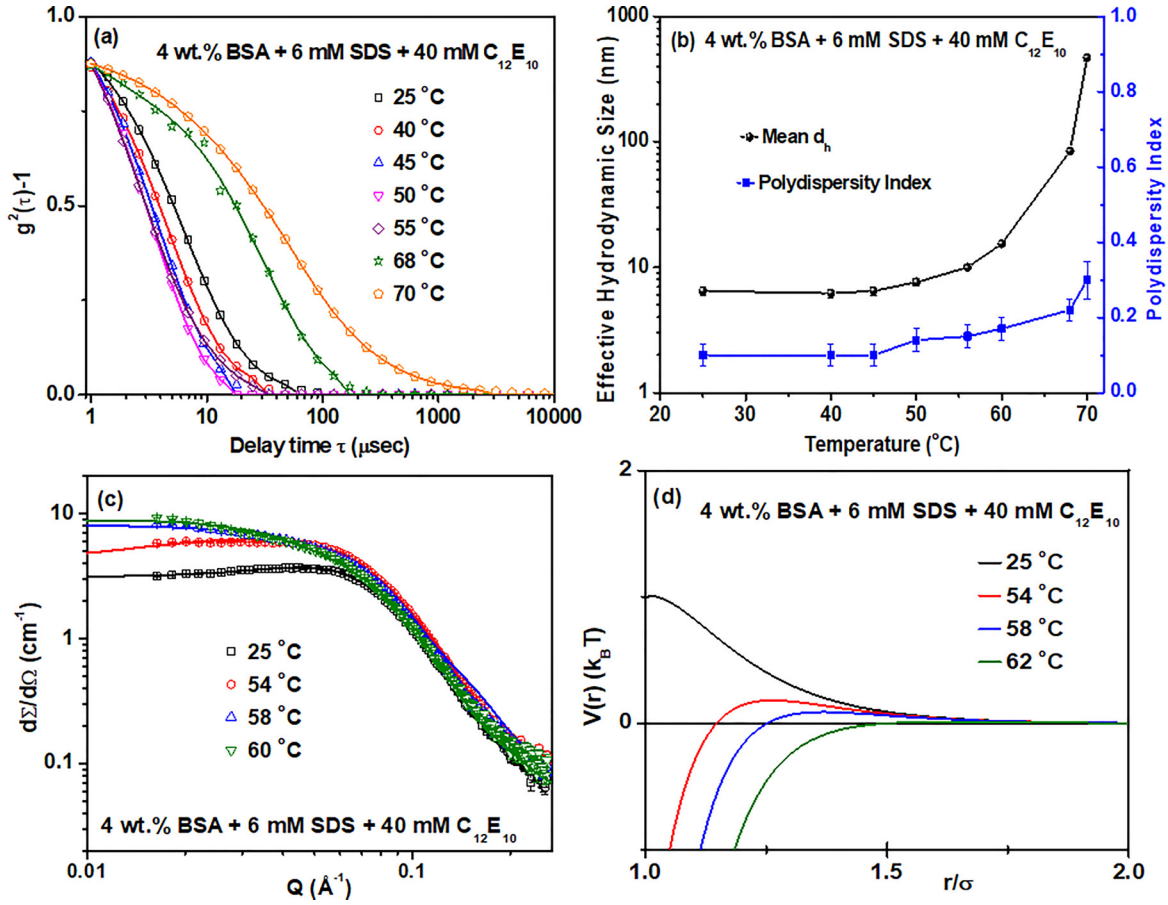

FIG. 5. (a) ACFs of the 4 wt % BSA+ 6 mM SDS+40 mM $C_{12}E_{10}$ system as measured by DLS with increasing temperature, (b) variation in the effective hydrodynamic size (d_h) and polydispersity index with increasing temperature as calculated using the DLS data presented in (a), (c) SANS data of the 4 wt % BSA+6 mM SDS +40 mM $C_{12}E_{10}$ system with increasing temperature, and (d) fitted total interaction potentials between protein molecules with rise in temperature.

TABLE III. Fitted parameters for 4 wt % BSA + 6 mM SDS + 40 mM $C_{12}E_{10}$ system with increasing temperature. The parameters for the mixed micelles have been kept fixed as obtained from Table ST2 [54]. The parameters of the repulsion were also kept fixed equivalent to those obtained from pure 4 wt % BSA solution at 25° C.

Temperature (°C)	Semimajor axis $b = c$ (nm)	Semiminor axis a (nm)	K_1 (k_BT)	Z_1	K_2 (k_BT)	Z_2
25	4.2 ± 0.3	1.4 ± 0.1	3.0 ± 0.3	6.0 ± 0.5	2.0 ± 0.2	10.0 ± 0.6
54	4.2 ± 0.3	1.4 ± 0.1	3.0 ± 0.3	6.0 ± 0.5	5.4 ± 0.2	10.0 ± 0.5
58	4.8 ± 0.3	1.4 ± 0.1	3.0 ± 0.3	6.0 ± 0.5	8.6 ± 0.3	10.0 ± 0.5
62	5.4 ± 0.3	1.5 ± 0.1	3.0 ± 0.3	6.0 ± 0.5	10.4 ± 0.3	8.5 ± 0.3

decay times, evidencing the formation of the larger structures of the protein aggregates, indicating the initiation of sol-gel transition.

To understand the role of $C_{12}E_{10}$ in tuning the sol state of 4 wt % BSA + 10 mM SDS to gel state, SANS measurements have been carried out. First, the SANS data of the 6 mM SDS + 40 mM $C_{12}E_{10}$ system have been compared with those of pure 40 mM $C_{12}E_{10}$ (Fig. S6 in SM [54]). The SANS data of the pure $C_{12}E_{10}$ do not show any correlation peak. Hence data have been fitted considering the form factor [$P(Q)$] for micelles consisting of a spherical core attached to the Gaussian chains (described in Ref. [45]) and $S(Q)$ approximated to unity. The fitting provides a micellar core radius of about 1.7 nm with a radius of gyration of the attached chains around 1.2 nm (Table ST1 in SM [54]). On the other hand, the SANS data of the 6 mM SDS + 40 mM $C_{12}E_{10}$ system shows a correlation peak, indicating the formation of interacting mixed micelles of SDS and $C_{12}E_{10}$. The SDS monomers are incorporated in the $C_{12}E_{10}$ micelles with the tail remaining in the micellar core and the head in the hydrophilic shell region, providing charge to the otherwise uncharged $C_{12}E_{10}$ micelles. The data analysis shows an increase in the micellar size, compared to that of the pure $C_{12}E_{10}$ micelles, and an effective charge of about 2.4 e.u. on the mixed micelles (Table ST2 in SM [54]). On increasing temperature, the size as well as the charge on the micelles increases due to enhanced hydrophobicity and counterion dissociation, respectively.

The SANS data [Fig. 5(c)] of 4 wt % BSA + 6 mM SDS + 40 mM $C_{12}E_{10}$ could be well fitted by considering the coexistence of BSA with free mixed micelles [Eq. (10)]. The fitted parameters are listed in Table III. In the fitting, the parameters of the mixed micelles have been kept fixed as obtained from SANS data (Fig. S6 and Table ST2 in SM [54]) of the 6 mM SDS + 40 mM $C_{12}E_{10}$ sample. On the other hand, $P(Q)$ of oblate ellipsoidal shape and $S(Q)$ of 2Y potential have been used to model the structure and interaction of BSA. This is consistent with the other reports, where the coexistence of such mixed micelles with protein has been utilized for refolding back the unfolded proteins [29,31–33]. The SDS monomers prefer to bind with $C_{12}E_{10}$ to form mixed micelles instead of binding with BSA, probably because the incorporation of SDS in $C_{12}E_{10}$ can reduce its exposure to water to a greater extent. In this way, hydrophobic interaction-driven mixed micellization of ionic and nonionic surfactants dominates over the charge-driven binding of the ionic surfactant with protein. This suggests that the interaction of SDS with BSA can be suppressed via the formation of mixed micelles with a nonionic surfactant, provided the nonionic surfactant should be noninteracting with protein [33]. The presence of $C_{12}E_{10}$ in sufficient amounts (more than six times that of SDS) ensures the release of the SDS from BSA and forms mixed SDS + $C_{12}E_{10}$ micelles, leaving the protein conformation unchanged.

On increasing the temperature, the data of the 4 wt % BSA + 6 mM SDS + 40 mM $C_{12}E_{10}$ system show an increase in the low-Q region, exhibiting the evolution of attractive interaction [Fig. 5(c)] in the system, similar to that observed for pure BSA. The fitted total potentials between protein molecules have been shown in Fig. 5(d), where a clear transition from repulsive to the attractive system can be observed. Fig. 6 shows a summary of the sol or gel states of different samples on heating, along with the driving interaction potentials. It should also be noted that the 4 wt % BSA + 6 mM SDS + 40 mM $C_{12}E_{10}$ system is less attractive compared to pure BSA, even at higher temperature, probably due to the presence of the interacting charged micelles. This can explain the observed higher gelation temperature of the 4 wt % BSA + 6 mM SDS + 40 mM $C_{12}E_{10}$ system compared to the pure 4 wt % BSA. Overall, the present study shows how interprotein interactions (e.g., hydrophobic, electrostatic, etc.) can be manipulated using amphiphilic molecules to gain control over the protein gelation or even other phases (e.g., coacervation, aggregation, crystallization, etc.), in a broader aspect.

IV. CONCLUSIONS

Protein denaturation and gelation, as encountered in a wide range of applications, requires proper tuning and understanding of structure and interaction for its effective utilization. In this study, we have controlled heat-driven gelation of a model BSA protein utilizing its cooperative and noncooperative interactions with ionic and nonionic surfactants. The

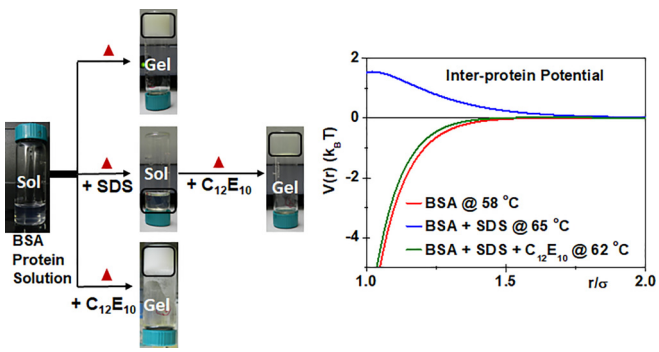

FIG. 6. Summary of the sol/gel states of different samples on heating, along with the comparison of the driving interaction potentials.

systems are studied under native conditions using small-angle neutron scattering, dynamic light scattering, and rheology. It has been shown that heat-induced protein gelation can be prevented via specific binding of the similarly charged surfactant (SDS) without altering the protein conformation. On the other hand, nonionic surfactant ($C_{12}E_{10}$), despite weak interaction with protein, supports protein gelation. The SDS-induced suppression of the protein gelation can be reversed by incorporating a nonionic surfactant in the system (unless the nonionic surfactant interacts with protein), where hydrophobic interaction-driven mixed micellization of ionic and nonionic surfactants dominates over the charge-driven binding of the ionic surfactant with protein. The results are explained using surfactant-induced modifications in interprotein interaction potentials. The interaction plots provide guidelines that can be selectively implemented to control protein denaturation and gelation by modifying physical interactions as per requirements. The idea of controlling the protein gelation is based on tuning the electrostatic and hydrophobic interactions. We believe that any ionic surfactant having (1) similar charge nature as that of protein and (2) affinity towards protein in the specific binding region can be used to suppress the protein gelation. Such suppression can be reversed by using a nonionic surfactant, in addition to the ionic surfactant. This nonionic surfactant should have strong interaction with the ionic surfactant but should not interact with the protein. Further studies will, however, be required to validate this for a combination of different globular proteins and surfactants.

ACKNOWLEDGMENT

The authors wish to thank Dr. Rajib Ganguly, Chemistry Division, BARC, for his help in rheology and viscosity measurements. The authors declare no conflict of interest.

[1] F. Mallamace, C. Corsaro, D. Mallamace, S. Vasi, C. Vasi, P. Baglioni, S. V. Buldyrev, S.-H. Chen, and H. E. Stanley, Energy landscape in protein folding and unfolding, Proc. Natl. Acad. Sci. USA **113**, 3159 (2016).

[2] E. A. Galpern, J. Marchi, T. Mora, A. M. Walczak, and D. U. Ferreiro, Evolution and folding of repeat proteins, Proc. Natl. Acad. Sci. USA **119**, e2204131119 (2022).

[3] A. Pastore, S. R. Martin, and P. A. Temussi, Generalized view of protein folding: In medio stat virtus, J. Am. Chem. Soc. **141**, 2194 (2019).

[4] D. Balchin, M. H.-Hartl, and F. U. Hartl, In vivo aspects of protein folding and quality control, Science **353**, 6294 (2016).

[5] T. Nicolai and C. Chassenieux, Heat-induced gelation of plant globulins, Curr. Opin. Food Sci. **27**, 18 (2019).

[6] Y. Cao and R. Mezzenga, Design principles of food gels, Nat. Food **1**, 106 (2020).

[7] Q. Bian, L. Fu, and H. Li, Engineering shape memory and morphing protein hydrogels based on protein unfolding and folding, Nat. Comm. **13**, 137 (2022).

[8] J. Kopeček and J. Yang, Smart self-assembled hybrid hydrogel biomaterials, Angew. Chem. Int. Ed. **51**, 7396 (2012).

[9] N. Amdursky, M. M. Mazo, M. R. Thomas, E. J. Humphrey, J. L. Puetzer, J.-P. St-Pierre, S. C. Skaalure, R. M. Richardson, C. M. Terracciano, and M. M. Stevens, Elastic serum-albumin based hydrogels: Mechanism of formation and application in cardiac tissue engineering, J. Mater. Chem. B **6**, 5604 (2018).

[10] E. van der Linden and E. A. Foegeding, Gelation: Principles, models and applications to proteins, in *Modern Biopolymer Science*, edited by S. Kasapis, I. T. Norton, and J. B. Ubbink (Academic, London, 2009), pp. 29–91.

[11] M. L. Floren, S. Spilimbergo, A. Motta, and C. Migliaresi, Carbon dioxide induced silk protein gelation for biomedical applications, Biomacromolecules **13**, 2060 (2012).

[12] S. Panja, A. Seddon, and D. J. Adams, Controlling hydrogel properties by tuning non-covalent interactions in a charge complementary multicomponent system, Chem. Sci. **12**, 11197 (2021).

[13] C. E. R. Edwards, D. J. Mai, S. Tang, and B. D. Olsen, Molecular anisotropy and rearrangement as mechanisms of toughness and extensibility in entangled physical gels, Phys. Rev. Mat. **4**, 015602 (2020).

[14] D. W. S. MacKenzie, A. Schaefer, J. Steckner, C. A. Leo, D. Naser, E. Artikis, A. Broom, T. Ko, P. Shah, M. Q. Ney *et al.*, A fine balance of hydrophobic-electrostatic communication pathways in a pH-switching protein, Proc. Natl. Acad. Sci. USA **119**, e2119686119 (2022).

[15] M. Alrosan, T.-C. Tan, A. M. Easa, S. Gammoh, and H. M. Alu'datt, Molecular forces governing protein-protein interaction: Structure-function relationship of complexes protein in the food industry, Crit. Rev. Food Sci. Nutr. **62**, 4036 (2022).

[16] X. D. Sun and S. D. Arntfield, Molecular forces involved in heat-induced pea protein gelation: Effects of various reagents on the rheological properties of salt-extracted pea protein gels, Food Hydrocolloids **28**, 325 (2012).

[17] J. H. Kim, N. V. Varankovich, A. K. Stone, and M. T. Nickerson, Nature of protein-protein interactions during the gelation of canola protein isolate networks, Food Res. Int. **89**, 408 (2016).

[18] W. S. Gosal and S. B. Ross-Murphy, Globular protein gelation, Curr. Opin. Colloid Interface Sci. **5**, 188 (2000).

[19] S. Kumar, I. Yadav, D. Ray, D. Saha, S. Abbas, V. K. Aswal, and J. Kohlbrecher, Evolution of interactions in the protein solution as induced by mono and multivalent ions, Biomacromolecules **20**, 2123 (2019).

[20] S. Kumar, D. Saha, D. Ray, S. Abbas, and V. K. Aswal, Unusual stability of protein molecules in the presence of multivalent counterions, Phys. Rev. E **104**, L012603 (2021).

[21] C. Chen, Y. Gu, L. Deng, S. Han, X. Sun, Y. Chen, J. R. Lu, and H. Xu, Tuning gelation kinetics and mechanical rigidity of β-hairpin peptide hydrogels via hydrophobic amino acid substitutions, ACS Appl. Mater. Interfaces **6**, 14360 (2014).

[22] P. Dubey, S. Kumar, V. K. Aswal, S. Ravindranathan, P. R. Rajamohanan, A. Prabhune, and A. Nisal, Silk fibroin-sophorolipid gelation: Deciphering the underlying mechanism, Biomacromolecules **17**, 3318 (2016).

[23] O. S. Nnyigide and K. Hyun, The protection of bovine serum albumin against thermal denaturation and gelation by sodium dodecyl sulfate studied by rheology and molecular dynamics simulation, Food Hydrocolloids **103**, 105656 (2020).

[24] K. A. Black, D. Priftis, S. L. Perry, J. Yip, W. Y. Byun, and M. Tirrell, Protein encapsulation via polypeptide complex coacervation, ACS Macro Lett. **3**, 1088 (2014).
[25] R. B. Singh, S. Mahanta, and N. Guchhait, Destructive and protective action of sodium dodecyl sulphate micelles on the native conformation of bovine serum albumin: A study by extrinsic fluorescence probe 1-hydroxy-2-naphthaldehyde, Chem. Phys. Lett. **463**, 183 (2008).
[26] Y. Li and J.-S. Lee, Staring at protein-surfactant interactions: Fundamental approaches and comparative evaluation of their combinations—A review, Anal. Chim. Acta **1063**, 18 (2019).
[27] T. Wang, X. Fan, J. Xu, R. Li, X. Yan, S. Liu, X. Jiang, F. Li, and J. Liu, Giant proteinosomes as scaffolds for light harvesting, ACS Macro Lett. **8**, 1128 (2019).
[28] D. Saha, D. Ray, S. Kumar, J. Kohlbrecher, and V. K. Aswal, Interaction of a bovine serum albumin (BSA) protein with mixed anionic–cationic surfactants and the resultant structure, Soft Matter **17**, 6972 (2021).
[29] D. Otzen, Protein–surfactant interactions: A tale of many states, Biochim. Biophys. Acta Proteins Proteomics **1814**, 562 (2011).
[30] D. Winogradoff, S. John, and A. Aksimentiev, Protein unfolding by SDS: The microscopic mechanisms and the properties of the SDS-protein assembly, Nanoscale **12**, 5422 (2020).
[31] S. Mehan, V. K. Aswal, and J. Kohlbrecher, Tuning of protein-surfactant interaction to modify the resultant structure, Phys. Rev. E **92**, 032713 (2015).
[32] D. Saha, D. Ray, J. Kohlbrecher, and V. K. Aswal, Unfolding and refolding of protein by a combination of ionic and nonionic surfactants, ACS Omega **3**, 8260 (2018).
[33] J. D. Kaspersen, A. Søndergaard, D. J. Madsen, D. E. Otzen, and J. S. Pedersen, Refolding of SDS-unfolded proteins by nonionic surfactants, Biophys. J **112**, 1609 (2017).
[34] J. D. Schmit, J. J. Bouchard, E. W. Martin, and T. Mittag, Protein network structure enables switching between liquid and gel states, J. Am. Chem. Soc. **142**, 874 (2020).
[35] J. R.-Franco, F. Camerin, N. Gnan, and E. Zaccarelli, Tuning the rheological behavior of colloidal gels through competing interactions, Phys. Rev. Mat. **4**, 045601 (2020).
[36] S. F. Santos, D. Zanette, H. Fischer, and R. Itri, A systematic study of bovine serum albumin (BSA) and sodium dodecyl sulfate (SDS) interactions by surface tension and small angle x-ray scattering, J. Colloid Interface Sci. **262**, 400 (2003).
[37] S. Kerstens, B. S. Murray, and E. Dickinson, Confocal microscopy of heat-induced aggregation and gelation of β-lactoglobulin in presence of non-ionic surfactant, Food Hydrocolloids **19**, 625 (2005).
[38] X. Wu, J. Hou, M. Li, J. Wang, D. L.Kaplan, and S. Lu, Sodium dodecyl sulfate-induced rapid gelation of silk fibroin, Acta Biomater. **8**, 2185 (2012).
[39] V. K. Aswal and P. S. Goyal, Small-angle neutron scattering diffractometer at Dhruva reactor, Curr. Sci. **79**, 947 (2000).
[40] C. J. Glinka, J. G. Barker, B. Hammouda, S. Krueger, J. J. Moyer, and W. J. Orts, The 30 m small-angle neutron scattering instruments at the national institute of standards and technology, J. Appl. Cryst. **31**, 430 (1998).
[41] P. A. Hassan, S. Rana, and G. Verma, Making sense of Brownian motion: Colloid characterization by dynamic light scattering, Langmuir **31**, 3 (2015).
[42] R. Pecora, *Dynamic Light Scattering* (Plenum, New York, 1985).
[43] D. I. Svergun and M. H. J. Koch, Small-angle scattering studies of biological macromolecules in solution, Rep. Prog. Phys. **66**, 1735 (2003).
[44] J. S. Pedersen, Analysis of small-angle scattering data from colloids and polymer solutions: Modeling and least-squares fitting, Adv. Colloid Interface Sci. **70**, 171 (1997).
[45] J. S. Pedersen, Form factors of block copolymer micelles with spherical, ellipsoidal and cylindrical cores, J. Appl. Crystallogr. **33**, 637 (2000).
[46] Y. Liu, E. Fratini, P. Baglioni, W.-R. Chen, and S.-H. Chen, Effective Long-Range Attraction between Protein Molecules in Solutions Studied by Small Angle Neutron Scattering, Phys. Rev. Lett. **95**, 118102 (2005).
[47] S. Kumar, I. Yadav, V. K. Aswal, and J. Kohlbrecher, Structure and interaction of nanoparticle-protein complexes, Langmuir **34**, 5679 (2018).
[48] Y. Liu, W.-R. Chen, and S.-H. Chen, Cluster formation in two-Yukawa fluids, J. Chem. Phys. **122**, 044507 (2005).
[49] S. Kumar, V. K. Aswal, and J. Kohlbrecher, Size-dependent interaction of silica nanoparticles with different surfactants in aqueous solution, Langmuir **28**, 9288 (2012).
[50] S. H. Arabi, B. Aghelnejad, C. Schwieger, A. Meister, A. Kerth, and D. Hinderberger, Serum albumin hydrogels in broad ph and temperature ranges: Characterization of their self-assembled structures and nanoscopic and macroscopic properties, Biomater. Sci. **6**, 478 (2018).
[51] M. A.da Silva and E. P. G. Arêas, Solvent-induced lysozyme gels: Rheology, fractal analysis, and sol-gel kinetics, J. Colloid Interface Sci. **289**, 394 (2005).
[52] O. S. Nnyigide and K. Hyun, Effects of anionic and cationic surfactants on the rheological properties and kinetics of bovine serum albumin hydrogel, Rheol. Acta **57**, 563 (2018).
[53] A. D. Nielsen, K. Borch, and P. Westh, Thermal stability of *Humicola insolens* cutinase in aqueous SDS, J. Phys. Chem. B **111**, 2941 (2007).
[54] See Supplemental Material at http://link.aps.org/supplemental/10.1103/PhysRevMaterials.7.015601 for additional experimental SANS and DLS data and fitted parameters.
[55] R. Laishram, S. Sarkar, I. Seth, N. Khatun, V. K. Aswal, U. Maitra, and S. J. George, Secondary nucleation-triggered physical cross-links and tunable stiffness in seeded supramolecular hydrogels, J. Am. Chem. Soc. **144**, 11306 (2022).
[56] I. Yadav, S. Kumar, V. K. Aswal, and J. Kohlbrecher, Structure and interaction in the pH-dependent phase behavior of nanoparticle-protein systems, Langmuir **33**, 1227 (2017).
[57] C. Hojgaard, H. V. Sorensen, J. S. Pedersen, J. R. Winther, and D. E. Otzen, Can a charged surfactant unfold an uncharged protein? Biophys. J **115**, 2081 (2018).